Methyl selenol as precursor in selenite reduction to Se/S species by methane-oxidizing bacteria

Eswayaha, A. S.; Hondow, N.; Scheinost, A. C.; Merroun, M.; Romero-Gonzalez, M.; Smith, T. J.; Gardiner, P. H. E.;

Originally published:

November 2019

Applied and Environmental Microbiology 85(2019)22, e01379-19

DOI: https://doi.org/10.1128/aem.01379-19

Selenite Reduction by Methane-oxidizing Bacteria: Methyl Selenol as Precursor for Methylated Se/S Species and Characterization of $Se_{8-x}S_x$ Nanoparticles

Abdurrahman S. Eswayah[1,2], Nicole Hondow[3], Andreas C. Scheinost[4], Mohamed Merroun[5], Maria Romero-González[6], Thomas J. Smith[1] and Philip H. E. Gardiner[1*]

[1]*Biomolecular Sciences Research Centre, Sheffield Hallam University, Sheffield, UK*

[2]*Biotechnology Research Centre, Tripoli, Libya*

[3] *School of Chemical and Process Engineering, University of Leeds, Leeds, UK*

[4]*The Rossendorf Beamline at ESRF, F-38043 Grenoble, France, and Institute of Resource Ecology, Helmholtz Zentrum Dresden Rossendorf, D-01328 Dresden*

[5]*Department of Microbiology, University of Granada, Granada, Spain*

[6] *School of Engineering and Materials Science (SEMS),Queen Mary University of London, Mile End Road, London E1 4NS.*

[*] To whom correspondence should be addressed: Biomolecular Sciences Research Centre, Sheffield Hallam University, Sheffield, S11WB, UK.

E-mail: p.h.gardient@shu.ac.uk

Summary

A wide range of microorganisms have been shown to transform selenium-containing oxyanions to reduced forms of the element, particularly selenium-containing nanoparticles. Such reactions are promising for detoxification of environmental contamination and production of valuable selenium-containing products such as nanoparticles for application in biotechnology. It has previously been shown that aerobic methane-oxidising bacteria, including *Methylococcus capsulatus* (Bath), are able to perform methane-driven conversion of selenite (SeO_3^{2-}) to selenium-containing nanoparticles and methylated selenium species. Here, the biotransformation of selenite by *Mc. capsulatus* (Bath) has been studied in detail

via a range of imaging, chromatographic and spectroscopic techniques. The results indicate that the nanoparticles are produced extracellularly and have a composition distinct from nanoparticles previously observed from other organisms. The spectroscopic data from the methanotroph-derived nanoparticles are best accounted for by a bulk structure composed primarily of octameric rings in the form $Se_{8-x}S_x$ with an outer coat of cell-derived biomacromolecules. Among a range of volatile methylated selenium and selenium-sulfur species detected, methyl selenol (CH_3SeH) was found only when selenite was the starting material, although selenium nanoparticles (both biogenic and chemically produced) could be transformed into other methylated selenium species. This result is consistent with methyl selenol being an intermediate in methanotroph-mediated biotransformation of selenium to all the methylated and particulate products observed.

Keywords: Selenite reduction, Elemental selenium, Methane-oxidizing bacteria, Mixed chalcogenide amorphous nanoparticles

Introduction

A key biotransformation mechanism of most microorganisms exposed to selenium oxyanions is dissimilatory reduction to nanoparticulate elemental selenium (Lortie *et al.*, 1992; Kessi *et al.*, 1999; Prakash *et al.*, 2009; Nancharaiah & Lens, 2015b). The formation of the nanoparticles (NPs) reduces the toxicity and bioavailability of the selenium species (Combs *et al.*, 1996; Nancharaiah & Lens, 2015a; Eswayah *et al.*, 2016; Song *et al.*, 2017; Vogel *et al.*, 2018). Not only does the formation of the NPs reduce the adverse environmental impact of the oxyanions on the microorganisms and their surroundings but present an approach that can potentially be harnessed to produce selenium NPs tailor-made for a variety of technological, clinical, analytical and industrial applications (Prasad, 2009; T. Wang *et al.*, 2010; Bai *et al.*, 2011; Tian *et al.*, 2012; Iranifam *et al.*, 2013; Ren *et al.*, 2013; Tran & Webster, 2013; J. Wang *et al.*, 2014; Ramya *et al.*, 2015; Jain *et al.*, 2016; Wadhwani *et al.*, 2016). However, made-to-order NPs with microbial intervention can only be achieved when the structural features of the NPs produced by the different bacteria are better understood and characterised.

In their 2004 paper, Oremland et al investigated the structural features of selenium nanospheres produced by Se-respiring bacteria (Oremland *et al.*, 2004). They found that the three bacteria studied produced red amorphous Se NPs with distinct features, two contained predominantly Se_6 chain units, and the third had Se_8 ring units. Hu and Barton found in an investigation into the reduction of selenium oxyanions by *Desulfovibrio desufuricans,* a sulfate-reducing bacterium, that amorphous spherical submicro particles containing selenium and sulfur were produced both inside and outside the cell. They found that the bacterium was more effective at reducing selenite. The authors also proposed the mechanisms by which the particles were formed (Hu and Barton, 2013). More recently, Vogel et al proposed that the biogenic selenium NPs produced by *Azospirillum brasilense* from the biotransformation of selenite is cyclic $Se_{8-n}S_n$ with Se_6S_2 the most likely structure (Vogel *et al.*, 2018). Tugarova et al reported the characterisation of amorphous selenium particles produced by *Azospirillum thiophilum* and found the presence of only selenium with no evidence of either Se-S or S-S bands in the Raman spectrum (Tugarova *et al.*, 2017). Moreover, Ruiz-Fresneda et al (2018), described the ability of *Stenotrophomonas bentonitica* for biogenic reduction of Se(IV), production of amorphous Se^0 (a-Se) nanospheres and their subsequent transformation to one-dimensional (1D) trigonal selenium (t-Se) nanostructure where sulfur was associated with the SeNPs. In our study, Eswayah et al, we presented indirect evidence from transmission electron microscopy (TEM) imaging with energy dispersive X-ray spectrometry (EDX) measurements to show that sulfur was associated with amorphous selenium in the extracellular NPs that are produced from the reduction of selenite by methane-oxidizing bacteria (Eswayah *et al.*, 2017).

Besides the above-mentioned studies on the biotransformation of selenium oxyanions most investigations have focused on the formation of the NPs. A few others have identified concomitant release of volatile selenium species into the headspace gas (Chasteen, 1993; Burra *et al.*, 2010). However, none of these approaches has provided enough information to enable the elucidation of the processes leading to the formation of the amorphous NPs. Indeed, the formation of the extracellular amorphous NPs forms as reported in many studies (Oremland *et al.*, 2004; T. Wang *et al.*, 2010; Dhanjal & Cameotra, 2010; Zhang *et al.*, 2012; Kamnev *et al.*, 2017) may indicate limited direct involvement of the microorganisms in their formation. In our experiments, we observed the size of the extracellular nanoparticles increases with time, which suggests that the growth of the NPs is a result of abiotic reactions in the culture medium outside the cells. The formation of mixed chalcogenide species by

exchange reactions, when both Se and S species are present in the gaseous and solution phase, has been reported (Meija & Caruso, 2004; Vriens *et al.*, 2015). It is probable that similar reactions occur in the culture medium solution resulting eventually to the formation of the nanoparticles.

In order to gain a better understanding of the biotic and abiotic transformations occurring in the culture, both selenium- and sulfur-containing species were sampled from the headspace and solution of selenite amended and control samples at fixed times by sorptive extraction in conjunction with analysis by thermal desorption - gas chromatography- mass spectrometry (TD-GC-MS) to identify the compounds. In parallel, the formed NPs were characterised by a range of physical techniques, namely; attenuated total reflectance Fourier transformation infrared spectroscopy (ATR-FTIR), Raman spectroscopy, transmission electron microscopy (TEM) and energy dispersive X-ray (EDX) spectrometry, X-ray absorption spectroscopy (XAS), and X-ray photoelectron spectroscopy (XPS). Herein, the results obtained from these measurements are used to inform the formation and elucidation of the structure of the sulfur-doped red amorphous selenium NPs produced when the methane-oxidizing bacterium *Methylococcus capsulatus* (Bath) reduces selenite.

Results

Preliminary investigations with the methanotroph species *Mc.capsulatus* (Bath) showed that the sizes of the NPs grew rapidly from an average of 220 ±51 nm in the first 4 hrs to about 400 ±77 nm in the next 44 hrs as previously published (Eswayah *et al.*, 2017). It is evident from the HAADF-STEM imaging and TEM thin-section micrographs of the nanoparticles produced by the bacterium that the NPs are associated extracellularly with the cells (see Fig. 1a). Furthermore, Se and S distributions in the EDX maps overlap, indicative of a spatial and likely structural association, suggesting the formation of mixed chalcogenide nanoparticles (see Fig.1b). The intensity of the Se signals was, however, much higher than that for S (see Fig. 1c). In addition, examination of the $S_{k\alpha}$ map reveals that not only was there sulfur in the particles but there was a trail of the element linking the particles to likely sulfur-containing proteins from the bacterial cells.

Se K-edge X-ray Absorption Near-Edge Structure (XANES) spectra of the particles formed by *Mc. capsulatus* (not shown) are in line with those of red amorphous Se with no detectable residual selenite present in the samples. Shell fitting of the Extended X-ray Absorption Fine-

Structure (EXAFS) spectra showed the characteristics of red elemental Se^0, with a Se-Se path at a distance of 2.35Å. A second Se-Se shell was detected at 3.69Å with coordination numbers less than what has been previously been observed for amorphous Se (Scheinost & Charlet, 2008; Scheinost *et al.*, 2008), possible indication for the presence of a mixed Se/S phase. This small coordination number cannot be attributed to the NP size far above 10 nm, nor to a high structural disorder, the Debye-Waller factor (σ^2) of this second Se-Se showed increasing structural order with particle growth over time, without increasing the respective coordination numbers (see Eswayah et al (2017) for a detailed discussion of these results). The small coordination numbers hence suggest the presence of (more weakly backscattering) S atoms, but attempts to establish their presence by shell fitting failed because of strong destructive interference between Se-Se and Se-S paths.

In order to unravel the make-up of the nanoparticles, the surfaces of the particles were characterized by FTIR, XPS and Raman spectroscopy.

FTIR Analysis

The FTIR spectra of the freeze-dried selenium nanoparticles produced by the *Mc. capsulatus* in liquid NMS medium amended with selenite, the Chem-NPs and the bacterial biomass are shown in Figure 2. The assigned bands are summarised in Table 1.

XPS analysis of the particle surface

The surface composition of the harvested red particles was obtained by XPS, and the elemental content are summarised in Figure 3a. In addition to the selenium which is present at a concentration of 1.25 Atomic weight%, there are five other elements: carbon (46.32%), oxygen (31.41%), nitrogen (8.61%), calcium (5.89%) and phosphorus (4.77%) that were detected on the surface of the particles. The presence of the first three elements is an indication that there are organic molecules on the particle surfaces. The high resolution spectra scans for Se, C, N, and O, and the assigned chemical species from the core level XPS spectra of C1s, N 1s, O 1s bands are shown in Figures 3b-e. The spectrum for 3d Se shows a doublet which is unresolved. However, the fitted deconvoluted peaks show two predominant bands at 55.16 and 56.02 binding energy (eV), and two minor peaks at 55.75 and 56.61 eV, respectively, the later pair of peaks resulting from the Se 3d peak split by spin orbit coupling into Se 3d5/2 and Se 3d3/2. The observed range of binding energies between 55.16 and

147 56.61eV is indicative of the presence of reduced selenium species, including elemental
148 selenium (Naveau *et al.*, 2007).

149 **Raman characterisation of the amorphous particles**

150 Vibrational spectroscopy particularly Raman spectroscopy has been the technique of choice
151 for the characterisation of Se_n allotropes, and aggregates. The deconvoluted spectrum
152 obtained between 50-600 cm^{-1} Raman shift from the harvested SeNPs is shown in Fig 4.
153 There are four bands which are visible: the main band at 251.5 cm^{-1} and smaller ones at 80.2,
154 358.8 and 506.5 cm^{-1}, respectively. All of the bands were present in all of the scans of
155 samples collected at different time points: 6, 24 and 48h. The band at 513.5 cm^{-1} was more
156 prominent than that at 358.8 cm^{-1}. The band at 80.2 cm^{-1}, which is a shoulder, is only visible
157 in the deconvoluted spectrum.

158 **Speciation of selenium and sulfur in the medium solution and headspace**

159 The GC-MS chromatograms of the species found in both the headspace and solution of the
160 selenite amended medium at 4h and 20h are shown in Figures 5 and 6, respectively. The
161 earlier time was chosen because the formation of the particles and therefore the red colour of
162 the solution were barely discernible. A summary of the selenium- and sulfur-containing
163 species are given in Table 3. Examination of the data in the Tables showed that after 4h, three
164 compounds: methyl selenol (MSeH), dimethyl selenenyl sulfide (DMSeS) and dimethyl
165 diselenide (DMDSe) were detected in both the solution and headspace. In addition dimethyl
166 diselenenyl sulfide (DMDSeS) was also found in the solution. At 20h, three new species:
167 Bis(methylselenomethane) (DMSe), dimethyl selenenyl disulfide (DMSeDS), and dimethyl
168 diselenenyl sulfide (DMDSeS) were detected in the solution in addition to triselenothone/
169 dimethyltriselenide (DMTSe) which was detected in both the solution and headspace.

170 **Discussion**

171 The results from the kinetics experiments showed that there were increases in particles sizes
172 with incubation time leading us to hypothesize that much of the structure of the particles was
173 formed in the extracellular space. If this is true, then the key reactions resulting in the
174 increase in the particle sizes are essentially abiotic in nature. Consequently, the clues to the
175 structural formation of the particles must lie in the nature and identity of the compounds that
176 are concomitant in the solution and headspace of the nascent particles. It was therefore

177 essential to sample for selenium- and sulfur-containing compounds in both the headspace and
178 solution, followed by their analyses and identification.

179
180 The FTIR spectra of the SeNPs produced by *Mc. capsulatus*, samples of biomass of the strain
181 (control), as well as the Chem-SeNPs were recorded in order to identify the functional groups
182 capping the synthesized SeNPs. The peak centred at 3297 cm^{-1} corresponds to the −OH and
183 −NH stretching vibrations of the amine and carboxylic groups. Peaks at 2927 cm^{-1}
184 corresponded to the aliphatic saturated C−H stretching modes (Naumann *et al*. 1995; Kamnev
185 *et al*. 2017). The peaks at 1644, 1538, and 1239 cm^{-1} are characteristic of amide I, amide II,
186 and amide III bands of proteins, respectively (Alvarez-Ordóñez *et al*. 2011; Ojeda & Dittrich
187 2012). The symmetrical stretch of carboxylate group can be attributed to the bands observed at
188 1366 cm^{-1}. The peaks at 1150, 1077 and 1015 cm^{-1} corresponded to the C−O stretching
189 vibrations of C-O-C groups (Naumann *et al*. 1995; Beekes *et al*. 2007). The presence of
190 phosphoryl groups was confirmed by the peak at 919 cm^{-1}. Additionally, peaks at 859 and 762
191 cm^{-1} (fingerprint region) could be mainly attributed to aromatic ring vibrations of aromatic
192 amino acids (tyrosine, tryptophan, phenylalanine) and possibly nucleotides (Burattini *et al*.
2008; Kamnev 2008).

193
194 The FTIR spectra of SeNPs of *Mc. capsulatus* differ from those of the bacterial biomass
195 (control) and the Chem-SeNPs. The main difference between the spectra is that the Bio-
196 SeNPs exhibit more peaks in the protein and polysaccharide vibration region, indicating the
197 presence of proteins and polysaccharides in the biomacromolecules capping the SeNPs
198 (Shirsat *et al.*, 2015; Wadhwani *et al.*, 2016; Tugarova & Kamnev, 2017; Kamnev *et al.*,
2017).

199
200 By contrast, Chem-SeNPs obtained through reaction of Na_2SeO_3 with L-cysteine displayed a
201 broad absorption band around 3350 cm^{-1} and absorption band at 2923 cm^{-1} that are assigned
202 to O−H vibrations of the absorbed H_2O and C−H vibration in the alkyl chain of L-cys,
203 respectively. The peak at 1606 cm^{-1}can be mainly attributed to C=O vibrations. It is
204 noteworthy that the presence of organic residues such as carbohydrates, lipids, and proteins on
205 the surface of biogenic SeNPs were completely absent in the Chem-SeNPs spectrum (see
206 Figure 2) FTIR spectra of the Bio-SeNPs separated from the *Mc. capsulatus* cells showed
207 bands typical of proteins, polysaccharides and lipids associated with the particles (in line with
208 their TEM images showing a thin layer over the particles), in addition to strong carboxylate
bands, which may stabilise the SeNPs structure and morphology.

The XPS results show two Se containing species, and other organic constituents.

In assigning the Se bands, it is essential to link the structure of the particles to the selenium-containing species that have been identified in the solution (see the discussion of the TD-GC-MS results below). Since data for the exact compounds are not available, structures that may be similar to these in the particles have been selected. The major band at 55.16 eV, has been assigned to the compound: $(CH_3)_2NC(Se)SeC(Se)N(CH_3)_2$ (Kobayashi *et al.*, 1986). This is a reasonable fit to the results obtained in this study not only because of the presence of selenium but also the content of the methyl groups and nitrogen. The nitrogen could account for the single band at 400.10eV usually assigned to amine nitrogen. The bands at 56.02 eV has been assigned to (-CSeC(CH_3)C(CH_3)Se-)2 (Dáaz *et al.*, 1996). Both of these assignments are an indication of the presence of long chain of selenium-containing methylated species. Missing from both spectra is oxygen which is presumably present as C=O, and either C-O-C or C-O-H at 531.58 and 532.84 eV, respectively.

However, the presence of Se-C was not detected in the spectrum thus indicating the amount of carbon directly bound to selenium was low. Furthermore, because of the high concentration of selenium in relation to sulfur, the signal for the latter could not be resolved and identified.

Whereas, both FTIR and XPS provided information on the forms in which the elements are present on the particle surface, Raman spectroscopy enables the identification of the basic structural make-up of the particles. It has been proposed that amorphous selenium is composed of a mixture of Se_n rings and helicoidal chains (Lucovsky *et al.*, 1967; Yannopoulos & Andrikopoulos, 2004; Demchenko *et al.*, 2010).The proportion of each depends on chemical and physical conditions under which the samples are made, and the treatments to which they have been subjected. According to Carini et al the band at around 250 cm^{-1} is characteristic of amorphous selenium (Carini *et al.*, 1980).The symmetrical band at 251.5 cm^{-1}, with full width half maxima of 30 cm^{-1} found in this study is characteristic of Se-Se stretching vibration in pure Se_8 (Lucovsky *et al.*, 1967; Baganich *et al.*, 1991; Nagels *et al.*, 1995) with its' deformation vibration at the deconvoluted band of 80.2 cm^{-1}. However, in the study of mixed selenium and sulfur alloys by Machado et al, the authors state that as the sulfur concentration increases in mixed amorphous selenium, the peak at 234 cm^{-1} usually associated with Se chains decreases in intensity and the band at 250 cm^{-1}, usually associated with selenium rings increases in intensity. They also observed the appearance of a band at

352 cm^{-1} as the selenium to sulfur ratio increases to either 4:1 or 7:3 (Machado *et al.*, 2010). The band at 358.8 cm^{-1} has been assigned to S-Se stretching vibration (Eysel & Sunder, 1979; Kasuya *et al.*, 1996). The band at 513.5 cm^{-1} is probably due to the Se-Se overtone band of the fundamental band at 251.5cm^{-1}. An important observation in this regard is that the S-S vibration band is not seen when the S composition is below that found in Se_6S_2 (Lucovsky *et al.*, 1967). Therefore it is probable that the composition of the harvested particles is Se_{8-x}, S_x , were x is equal to or greater than 2.

The intensity of the band 251.5 cm^{-1} is indicative of the predominance of the Se-Se bonds in the structure of the particles. It is probable that S is integral to the mixed particle structure $Se_{8-x}S_x$, and not as an S_8 impurity in the particles. The low available sulfur content in the medium makes the formation of an S-S homonuclear bond in the mixed particle structure highly unlikely (Eysel & Sunder, 1979).

We have previously reported that methyl selenol is produced and detected in the head space only when selenite is in the starting medium (Eswayah et al, 2017). Besides the presence of methyl selenol in the headspace, methyl selenoacetate was also detected. However, in the present study methyl selenoacetate was not detected when the headspace sorptive extraction probes were deployed for sample collection. No methyl selenol was detected when either the harvested or chemically synthesized nanoparticles were added to the medium in the absence of selenite. Therefore, we propose that methyl selenol may be the precursor of all of the methylated selenium species as well as the selenium-containing nanoparticles. If this is the case, the first step in the biotransformation of selenite would involve the reduction and methylation of selenite to methyl selenol followed by the formation of the other selenium- and sulfur-containing species. Indeed, the formation of some of the latter species requires the presence of the nascent selenium particles.

Based on these observations a possible pathway for the formation of the particles and the other products of biotransformation of selenite can be outline as in Scheme 1.

A series of abiotic reactions proposed by Ganther (1968; 1971) and outlined by Xu and Barton (2013) implicate glutathione (GSH) and GSH reductase in the production of elemental selenium. The proposed steps leading up to the formation of methyl selenol are shown in Scheme 2.

The presence of sulfur-containing species was detected in the headspace and culture supernatant of the control *Mc. capsulatus* culture without added selenite. These species included: benzothiazole, dodecanethiol, and propanesulfonyl, which are the likely source of sulfur in the structure of the particles. Evidence of the formation of the longer chains of the selenium- containing species can be seen in the nature of the compounds that are found in the solution after hours of incubation, first after 4h, dimethyl diselenenyl sulfide was detected, and subsequently dimethylselenodisulfide, dimethyltriselenide and bis(methylseleno) methane were detected after 20h. More complex mixed Se and S compounds are formed in the medium with time. The formation of the mixed chalcogenides of Se and S is hardly surprising since S may be available from the reduction of sulfate in the growth medium. A key question therefore is how the solution chemistry relates to the observed structural features of the Se particulates.

It is likely that these longer chains polymerize to form Se_x or $Se_{8-x}S_x$ linear or cyclic structures. Indeed, all chalogen elements have the tendency to form cyclic allotropes. The dominant allotrope will depend on the experimental conditions. Examples of exchange reactions that may occur based on the presence of the detected selenium- and sulfur-containing species are shown in the following equations:

-Se-Se- + 2-Se-Se-Se- ----->Se_8 (1)

-Se-S- + 2-Se-Se-Se- -----> Se_7S (2)

2-Se-Se-S- + -Se-Se- -----> Se_6S_2 (3)

As can be seen a variety of nanocomposites can be formed. Similar exchange reactions have been shown to occur when mixed Se and S complexes are present in the same solution (Vriens *et al.*, 2015). Indeed these reactions are known to occur in amorphous selenium semiconductors (Steudel, 1986). The Raman results indicate these are not open chains clusters but cyclic structures with the Se_8 structure dominant and the probable presence of small amounts of Se-S bonds. To prevent the introduction of sulfur into the structures, the presence of the element could be reduced from amount in the culture medium if this does not affect the bacterial growth.

The formed particles are surrounded and stabilized by the presence of polymeric substances as proposed by Jain *et al* (2015) as evidenced by the XPS and FTIR measurements.

In this study, we demonstrate for the first time that in the reduction of selenite by *Mc. capsulatus* (Bath), a methane oxidizing bacterium, methyl selenol is the likely precursor for the formation of methylated selenium-containing and mixed chalcogenides species. Subsequent exchange reactions between the species result in the formation of the amorphous allotropic form of selenium, cyclic Se_8 with sulfur in its structure. The nature of the molecular mediators in reduction of selenite, supplying sulfur that is integral to the structure of the nanoparticles and supplying the methyl groups found in the volatile selenium containing products remain to be identified.

Experimental Procedures

Bacterial strains and growth conditions

The methanotrophic bacterium *Methylococcus capsulatus* (Bath) (NCIBM 11132) was grown and propagated aerobically using methane as the carbon and energy source as previously described (Eswayah et al, 2017). For these experiments the initial selenite concentration used was 20 mg L^{-1}.

Detection of solution and volatile selenium species

Solution and volatile selenium-containing species were sampled by immersive sorptive extraction using sampling probes (HiSorb probe, Markes International, UK) from either the solution or headspace. Extension screw-on arms were fabricated for each probe so that they could be inserted through the Suba-Seals used to seal the necks of the culture flasks. To ensure that the probes and tubes were contamination free, before use, the probes and tubes were preconditioned with helium at flow rate of 90 mL min^{-1} using the following temperature programme: 15 min at 100 °C, 15 min at 200 °C, 15 min at 300 °C and 15 min at 335 °C. The preconditioned probes were inserted into either the liquid or headspace of the *Mc. capsulatus* (Bath) culture medium through the Suba-Seals. The probes were removed from the Suba-Seals after different incubation time (4 and 20 h, respectively), rinsed with HPLC grade water, dried with lint-free tissue, and then placed into the thermal desorption tubes (Markes International, UK).

Samples analyses were performed on a combined thermal desorption GC–MS system. The volatiles were desorbed at 250°C and concentrated on a thermal desorber (Unity®, Markes International Limited) at -10°C cold trap for 5 min (helium flow 50 mL min^{-1}) and then were transferred onto the GC/MS system (7890A-GC with 5975C-MS, Agilent Technologies) equipped with a capillary column (Agilent J&W HP- MS GC Column, 30 m, 0.25 mm, 0.25

μm). Helium was used as the carrier gas at a flow rate of 1 mL min^{-1}, injector temperature, 250°C, and the chromatogram was obtained using the following temperature programme: 35° C for 1 min; 10°C min^{-1} to 25 0°C; and then held at 25 0°C for 1 min. The National Institute of Standards and Technology (NIST) MS search program (version 2011) was used to identify the compounds based on their MS spectrum.

Extraction of selenium nanoparticles produced by *Mc. capsulatus* (Bath)

Freshly grown cultures (at OD_{600} of 0.5-0.8) were supplemented with 20 mg L^{-1} SeO_3^{2-} and incubation was continued at 45°C with shaking in the presence of methane. After 48h the development of the reddish colour had occurred, the cultures were pelleted by centrifugation (at 12,500 × *g*; 10 min). SeNPs were extracted by a modification of the method published by Sonkusre et al. (2014) , as follows. The resultant pellet was washed and re-suspended in 10 mL of sterile water followed by addition of lysozyme to give a final concentration of 500 μg mL^{-1}, and the tube was incubated at 37°C for 3 h. The suspension was passed through a French pressure cell (1500 psi, 4°C). The resultant slurry containing both cell debris and NPs was washed four times at 15,000 × *g* for 10 min with 1.5 M Tris-HCl (pH 8.3) containing 1% sodium dodecyl sulfate (SDS). The resultant pellet containing SeNPs and the insoluble cell wall fraction was washed and resuspended in 4 mL sterile water in a 15 mL Falcon tube, and 2 mL of 1-octanol were added. The solution was mixed vigorously on a vortex mixture for five min and centrifuged at 2000 × g for 5 min at 4°C. The tubes were then kept undisturbed at 4° C for 24 hours. The upper phase and interface containing the insoluble cell fraction were removed, and the bottom water phase containing SeNPs was transferred to a clean 15 mL centrifuge tube. This was washed sequentially with chloroform, absolute ethanol, 70% ethanol, and water at 16000 × *g*. Collected NPs were re-suspended in water and stored at 4°C.

Transmission electron microscopy (TEM) and energy dispersive X-ray (EDX) spectrometry/high-angle annular dark-field (HAADF) scanning TEM (STEM) analysis

Samples of selenite amended culture were treated and analysed as previously described (Eswayah et al, 2017). The samples were examined in an FEI Tecnai F20 field emission gun (FEG)-TEM operating at 200 kV and fitted with a Gatan Orius SC600A CCD camera, an Oxford Instruments XMax SDD EDX detector and a high-angle annular dark-field (HAADF) scanning TEM (STEM) detector.

For thin section analysis, after the ethanol dehydration steps, the cells were embedded in EM bed 812 epoxy resin and cut into thin sections (90 nm, using a diamond knife on a Reichert Ultracut S ultramicrotome). The sections were supported on copper grids and coated with

carbon. TEM specimen holders were cleaned by plasma prior to TEM analysis to minimize contamination. Samples were examined with a high-resolution Philips CM 200 transmission electron microscope at an acceleration voltage of 200 kV under standard operating conditions with the liquid nitrogen anti-contaminator in place.

X-ray absorption spectroscopy

The conditions for the X-ray absorption spectroscopy measurements were as described previously (Eswayah et al, 2017).

X-ray photoelectron spectroscopy (XPS) analysis

Harvested SeNPs samples were deposited on silicon wafer, left to dehydrate in the load lock of the XPS instrument overnight. The analyses were carried out using a Kratos Axis Ultra DLD instrument with the monochromated aluminium source. Survey scans were collected between1200 to 0eV binding energy, at 160 eV pass energy and 1 eV intervals. High-resolution C 1s, N 1s, O 1s, Se 3d and S 2p spectra were collected over an appropriate energy range at 20 eV pass energy and 0.1 eV intervals. The analysis area was 700 μm by 300 μm. Two areas were analysed for each sample, collecting the data in duplicate. Charge neutralisation was used with intention of preventing excessive charging of the samples during analysis. The data collected were calibrated in intensity using a transmission function characteristic of the instrument (determined using software from NPL) to make the values instrument independent. The data can then be quantified using theoretical Schofield relative sensitivity factors. The data were calibrated for binding energy using the main carbon peak C 1s at 285.0 as the reference peak, and correcting all data for each sample analysis accordingly.

Raman spectroscopy analysis of SeNPs

Aliquots of 2 μL of SeNPs suspended in water were transferred onto a calcium fluoride (CaF_2) slide and air-dried prior to Raman analysis. Raman spectra were obtained using a Horiba LabRam HR and a modified Horiba LabRam HR (Wellsens Biotech. Ltd., China). Three factors have been modified in this new Raman system to improve Raman spectral quality. These comprise shortening the Raman light path, employing a low noise and sensitive EMCCD for the Raman signal detection, and increasing incident laser power. The old and new modified systems are identical except these three factors. The Raman signals were collected by a Newton EMCCD (DU970N-BV, Andor, UK) utilizing a 1600 × 200 array of 16 μm pixels with thermoelectric cooling down to −70°C for negligible dark current. A 532 nm Nd:YAG laser (Ventus, Laser Quantum Ltd., UK) was used as the light source for Raman measurement. A 100× magnifying dry objective (NA = 0.90, Olympus, UK) was used for sample observation and Raman signal acquisition. A 600 line/mm grating was used for

the measurements, resulting in a spectral resolution of ~1 cm^{-1} with 1581 data points. The laser power on sample was measured by a laser power meter (Coherent Ltd.). The Raman spectra were processed by background subtraction (using spectra from cell free region on the same slide) and normalization using the Labspec5 software (HORIBA Jobin Yvon Ltd., UK).

Fourier transformation infrared (FT-IR) spectroscopy measurements of SeNPs

In order to determine the functional groups present on the SeNPs, the FTIR spectra of SeNPs were recorded on a PerkinElmer Spectrum 100 FT-IR Spectrometer equipped with an attenuated total reflectance (ATR) attachment. Spectra were recorded from 4,000 to 650 cm^{-1}, and 4 scans were averaged at a resolution of 4 cm^{-1}. Extracted SeNPs were freeze dried overnight and analyzed without further treatment. For comparison, the FTIR spectra of samples of bacterial cells (as control) and chemically synthesized SeNPs (Chem-SeNPs) were also recorded. For the controls, freshly grown cultures (OD_{600} ~ 0.7) of *Mc. capsulatus* (Bath) were centrifuged at 11000 × *g* for 10 min to obtain the cell pellets. The pellets were washed twice with phosphate buffered saline (Sodium chloride, 150 mM, and sodium phosphate, 150 mM) pH 7.2, and then freeze dried overnight. The synthesis of Chem-SeNPs was done according to the procedure of (Lampis *et al.*, 2017) as follows: 1.0 mL of 50 mM L-cysteine (Sigma-Aldrich, Dorset, UK) solution was added dropwise into 1.0 mL of 0.1 M Na_2SeO_3. The mixed solution was then stirred for 30 min at room temperature. The Chem-SeNPs were pelleted by centrifugation (at 15000 × *g*; 10 min), and then freeze dried overnight.

Acknowledgement

ASE is grateful for the award of a PhD scholarship from the Government of Libya.

Conflict of Interest

The authors declare no conflict of interest.

Originality-Significance Statement

We certify that all of the research and the conclusions are original and have not been presented elsewhere.

429 References

430 Baganich, A., Mikla, V., Semak, D., Sokolov, A., & Shebanin, A. (1991) Raman scattering in
431 amorphous selenium molecular structure and photoinduced crystallization. *physica*
432 *status solidi (b)* **166:** 297-302.

433 Bai, Y., Rong, F., Wang, H., Zhou, Y., Xie, X., & Teng, J. (2011) Removal of copper from
434 aqueous solutions by adsorption on elemental selenium nanoparticles. *Journal of*
435 *Chemical & Engineering Data* **56:** 2563-2568.

436 Burra, R., Pradenas, G. A., Montes, R. A., Vásquez, C. C., & Chasteen, T. G. (2010)
437 Production of dimethyl triselenide and dimethyl diselenenyl sulfide in the headspace of
438 metalloid-resistant bacillus species grown in the presence of selenium oxyanions. *Anal*
439 *Biochem* **396:** 217-222.

440 Carini, G., Cutroni, M., Fontana, M., Galli, G., & Migliardo, P. (1980) Resonant Raman
441 scattering in amorphous bulk selenium. *Solid State Commun* **33:** 1143-1145.

442 Chasteen, T. G. (1993) Confusion between dimethyl selenenyl sulfide and dimethyl selenone
443 released by bacteria. *Applied organometallic chemistry* **7:** 335-342.

444 Combs, G. F., Garbisu, C., Yee, B. C., Yee, A., Carlson, D. E., Smith, N. R. et al. (1996)
445 Bioavailability of selenium accumulated by selenite-reducing bacteria. *Biol Trace Elem*
446 *Res* **52:** 209-225.

447 Dáaz, F., Godoy, A., Tagle, L., Valdebenito, N., & Bernede, J. (1996) Poly (p-phenylene-
448 diselenocarbonate) and poly (p-phenylene-diselenothiocarbonate): New semiconducting
449 polymers. *European polymer journal* **32:** 1155-1160.

450 Demchenko, P. Y., Gladyshevskii, R. E., Volkov, S. V., Yanko, O. G., Kharkova, L. B.,
451 Fokina, Z. A., & Fokin, A. A. (2010) The first nonaselenium ring. *Chemical*
452 *Communications* **46:** 4520-4522.

453 Dhanjal, S., & Cameotra, S. S. (2010) Aerobic biogenesis of selenium nanospheres by
454 Bacillus cereus isolated from coalmine soil. *Microbial cell factories* **9:** 52.

455 Eswayah, A. S., Smith, T. J., Scheinost, A. C., Hondow, N., & Gardiner, P. H. (2017)
456 Microbial transformations of selenite by methane-oxidizing bacteria. *Appl Microbiol*
457 *Biotechnol* **101:** 6713-6724.

458 Eswayah, A. S., Smith, T. J., & Gardiner, P. H. (2016) Microbial Transformations of
459 Selenium Species of Relevance to Bioremediation. *Appl Environ Microbiol* **82:** 4848-
460 4859.

461 Eysel, H., & Sunder, S. (1979) Homonuclear bonds in sulfur-selenium mixed crystals: a
462 Raman spectroscopic study. *Inorg Chem* **18:** 2626-2627.

463 Ganther, H. E. (1971) Reduction of the selenotrisulfide derivative of glutathione to a
464 persulfide analog by gluthathione reductase. *Biochemistry (N Y)* **10:** 4089-4098.

Ganther, H. E. (1968) Selenotrisulfides. Formation by the reaction of thiols with selenious acid. *Biochemistry (N Y)* **7:** 2898-2905.

Iranifam, M., Fathinia, M., Rad, T. S., Hanifehpour, Y., Khataee, A., & Joo, S. (2013) A novel selenium nanoparticles-enhanced chemiluminescence system for determination of dinitrobutylphenol. *Talanta* **107:** 263-269.

Jain, R., Dominic, D., Jordan, N., Rene, E. R., Weiss, S., van Hullebusch, E. D. et al. (2016) Preferential adsorption of Cu in a multi-metal mixture onto biogenic elemental selenium nanoparticles. *Chem Eng J* **284:** 917-925.

Jain, R., Jordan, N., Weiss, S., Foerstendorf, H., Heim, K., Kacker, R. et al. (2015) Extracellular polymeric substances govern the surface charge of biogenic elemental selenium nanoparticles. *Environ Sci Technol* **49:** 1713-1720.

Kamnev, A. A., Mamchenkova, P. V., Dyatlova, Y. A., & Tugarova, A. V. (2017) FTIR spectroscopic studies of selenite reduction by cells of the rhizobacterium Azospirillum brasilense Sp7 and the formation of selenium nanoparticles. *J Mol Struct* **1140:** 106-112.

Kasuya, A., Watanabe, K., Takahashi, H., Toji, K., Motomiya, K., & Nishina, Y. (1996) Stability of SxSey ring clusters studied by Raman scattering. *Materials Science and Engineering: A* **217:** 12-14.

Kessi, J., Ramuz, M., Wehrli, E., Spycher, M., & Bachofen, R. (1999) Reduction of selenite and detoxification of elemental selenium by the phototrophic bacterium *Rhodospirillum rubrum*. *Appl Environ Microbiol* **65:** 4734-4740.

Kobayashi, K., Tukada, H., Kikuchi, K., & Ikemoto, I. (1986) NMR and XPS studies of some diselenocarbamates. Bond switch in bis (dimethylselenocarbamoyl) triselenide. *Bull Chem Soc Jpn* **59:** 1741-1746.

Lampis, S., Zonaro, E., Bertolini, C., Cecconi, D., Monti, F., Micaroni, M. et al. (2017) Selenite biotransformation and detoxification by Stenotrophomonas maltophilia SeITE02: novel clues on the route to bacterial biogenesis of selenium nanoparticles. *J Hazard Mater* **324:** 3-14.

Lortie, L., Gould, W. D., Rajan, S., McCready, R. G., & Cheng, K. J. (1992) Reduction of Selenate and Selenite to Elemental Selenium by a *Pseudomonas stutzeri* Isolate. *Appl Environ Microbiol* **58:** 4042-4044.

Lucovsky, G., Mooradian, A., Taylor, W., Wright, G., & Keezer, R. (1967) Identification of the fundamental vibrational modes of trigonal, α-monoclinic and amorphous selenium. *Solid State Commun* **5:** 113-117.

Machado, K., Dubiel, A., Deflon, E., Kostrzepa, I., Stolf, S., Sanchez, D., & Jóvári, P. (2010) Investigation on vibrational and structural properties of amorphous Se1− xSx alloys produced by mechanical alloying by Raman spectroscopy, X-ray diffraction, EXAFS and RMC simulations. *Solid State Commun* **150:** 1359-1363.

Meija, J., & Caruso, J. A. (2004) Selenium and sulfur trichalcogenides from the chalcogenide exchange reaction. *Inorg Chem* **43:** 7486-7492.

Nagels, P., Sleeckx, E., Callaerts, R., & Tichy, L. (1995) Structural and optical properties of amorphous selenium prepared by plasma-enhanced CVD. *Solid State Commun* **94:** 49-52.

Nancharaiah, Y. V., & Lens, P. N. (2015a) Selenium biomineralization for biotechnological applications. *Trends Biotechnol* **33:** 323-330.

Nancharaiah, Y. V., & Lens, P. N. (2015b) Ecology and biotechnology of selenium-respiring bacteria. *Microbiol Mol Biol Rev* **79:** 61-80.

Naveau, A., Monteil-Rivera, F., Guillon, E., & Dumonceau, J. (2007) Interactions of aqueous selenium (− II) and (IV) with metallic sulfide surfaces. *Environ Sci Technol* **41:** 5376-5382.

Oremland, R. S., Herbel, M. J., Blum, J. S., Langley, S., Beveridge, T. J., Ajayan, P. M. et al. (2004) Structural and spectral features of selenium nanospheres produced by Se-respiring bacteria. *Appl Environ Microbiol* **70:** 52-60.

Prakash, N. T., Sharma, N., Prakash, R., Raina, K. K., Fellowes, J., Pearce, C. I. et al. (2009) Aerobic microbial manufacture of nanoscale selenium: exploiting nature's bio-nanomineralization potential. *Biotechnol Lett* **31:** 1857.

Prasad, G. (2009) Biomedical applications of nanoparticles. In *Safety of nanoparticles.* Springer, pp. 89-109.

Ramya, S., Shanmugasundaram, T., & Balagurunathan, R. (2015) Biomedical potential of actinobacterially synthesized selenium nanoparticles with special reference to anti-biofilm, anti-oxidant, wound healing, cytotoxic and anti-viral activities. *Journal of Trace Elements in Medicine and Biology* **32:** 30-39.

Ren, Y., Zhao, T., Mao, G., Zhang, M., Li, F., Zou, Y. et al. (2013) Antitumor activity of hyaluronic acid–selenium nanoparticles in Heps tumor mice models. *Int J Biol Macromol* **57:** 57-62.

Ruiz-Fresneda, M. A. R., Martín, J. D., Bolívar, J. G., Cantos, M. V. F., Bosch-Estévez, G., Moreno, M. F. M., & Merroun, M. L. (2018) Green synthesis and biotransformation of amorphous Se nanospheres to trigonal 1D Se nanostructures: impact on Se mobility within the concept of radioactive waste disposal. *Environmental Science: Nano*

Scheinost, A. C., & Charlet, L. (2008) Selenite reduction by mackinawite, magnetite and siderite: XAS characterization of nanosized redox products. *Environ Sci Technol* **42:** 1984-1989.

Scheinost, A. C., Kirsch, R., Banerjee, D., Fernandez-Martinez, A., Zaenker, H., Funke, H., & Charlet, L. (2008) X-ray absorption and photoelectron spectroscopy investigation of selenite reduction by FeII-bearing minerals. *J Contam Hydrol* **102:** 228-245.

539 Shirsat, S., Kadam, A., Naushad, M., & Mane, R. S. (2015) Selenium nanostructures:
540 microbial synthesis and applications. *Rsc Advances* **5:** 92799-92811.

541 Song, D., Li, X., Cheng, Y., Xiao, X., Lu, Z., Wang, Y., & Wang, F. (2017) Aerobic
542 biogenesis of selenium nanoparticles by *Enterobacter cloacae* Z0206 as a consequence
543 of fumarate reductase mediated selenite reduction. *Scientific Reports* **7:** 3239.

544 Sonkusre, P., Nanduri, R., Gupta, P., & Cameotra, S. S. (2014) Improved extraction of
545 intracellular biogenic selenium nanoparticles and their specificity for cancer
546 chemoprevention. *Journal of Nanomedicine & Nanotechnology* **5:** 1.

547 Steudel, R. (1986) Hypervalent defects in amorphous selenium and similar lone-pair
548 semiconductors. *J Non Cryst Solids* **83:** 63-79.

549 Tian, B., Van den Bossche, J., & Kostarelos, K. (2012) Design and engineering of
550 multifunctional quantum dot-based nanoparticles for simultaneous therapeutic-diagnostic
551 applications. In *Multifunctional nanoparticles for drug delivery applications.* Springer,
552 pp. 345-365.

553 Tran, P. A., & Webster, T. J. (2013) Antimicrobial selenium nanoparticle coatings on
554 polymeric medical devices. *Nanotechnology* **24:** 155101.

555 Tugarova, A. V., & Kamnev, A. A. (2017) Proteins in microbial synthesis of selenium
556 nanoparticles. *Talanta* **174:** 539-547.

557 Tugarova, A. V., Mamchenkova, P. V., Dyatlova, Y. A., & Kamnev, A. A. (2017) FTIR and
558 Raman spectroscopic studies of selenium nanoparticles synthesised by the bacterium
559 *Azospirillum thiophilum*. *Spectrochimica Acta Part A: Molecular and Biomolecular*
560 *Spectroscopy* **192:** 458-463.

561 Vogel, M., Fischer, S., Maffert, A., Hübner, R., Scheinost, A., Franzen, C., & Steudtner, R.
562 (2018) Biotransformation and detoxification of selenite by microbial biogenesis of
563 selenium-sulfur nanoparticles. *J Hazard Mater* **344:** 749-757.

564 Vriens, B., Mathis, M., Winkel, L. H., & Berg, M. (2015) Quantification of volatile-alkylated
565 selenium and sulfur in complex aqueous media using solid-phase microextraction.
566 *Journal of Chromatography A* **1407:** 11-20.

567 Wadhwani, S. A., Shedbalkar, U. U., Singh, R., & Chopade, B. A. (2016) Biogenic selenium
568 nanoparticles: current status and future prospects. *Appl Microbiol Biotechnol* **100:** 2555-
569 2566.

570 Wang, J., Zhang, Y., Yuan, Y., & Yue, T. (2014) Immunomodulatory of selenium nano-
571 particles decorated by sulfated *Ganoderma lucidum* polysaccharides. *Food and chemical*
572 *toxicology* **68:** 183-189.

573 Wang, T., Yang, L., Zhang, B., & Liu, J. (2010) Extracellular biosynthesis and
574 transformation of selenium nanoparticles and application in H2O2 biosensor. *Colloids*
575 *and Surfaces B: Biointerfaces* **80:** 94-102.

576 Xu, H., & Barton, L. L. (2013) Se-bearing colloidal particles produced by sulfate-reducing
577 bacteria and sulfide-oxidizing bacteria: TEM study. *Advances in Microbiology* **3:** 205.

578 Yannopoulos, S., & Andrikopoulos, K. (2004) Raman scattering study on structural and
579 dynamical features of noncrystalline selenium. *J Chem Phys* **121:** 4747-4758.

580 Zhang, L., Li, D., & Gao, P. (2012) Expulsion of selenium/protein nanoparticles through
581 vesicle-like structures by Saccharomyces cerevisiae under microaerophilic environment.
582 *World Journal of Microbiology and Biotechnology* **28:** 3381-3386.

583

List of Figures

Figure1 TEM thin-section micrographs of *Mc. capsulatus* (a) exposed to 20 mg L^{-1} SeO_3^{2-}, showing the extracellular locations of the Se^0 nanospheres, HAADF-STEM imaging, showing Se nanospheres associated with the cells with EDX maps (generated from spectra collected from the indicated areas) of Se and S(b) and TEM of *Mc. capsulatus* cultures exposed to 20 mg L^{-1} SeO_3^{2-} (c) with EDX analysis within the electron dense regions (Se^0 nanospheres). Cells were fixed with 3% glutaraldehyde and 2% OsO_4 immediately before the analysis.

Figure 2 The FTIR spectra of freeze dried Bio-SeNPs (blue) and bacterial biomass (red) of *Mc. capsulatus* exposed to 20 mg L^{-1} SeO_3^{2-} and harvested at OD_{600} ~ 0.7, separated by centrifugation, washed with phosphate buffered saline pH 7.2 and freeze dried; as well as Chem-SeNPs (black) obtained through reaction of Na_2SeO_3 with L-cysteine. The spectra are representatives of 5 runs of the experiments.

Figure 3 Wide scan X-ray photoelectron spectra of the SeNPs produced by *Mc. capsulatus* (a) and high resolution spectra for Se 3d, C 1s, O 1s and N 1s are shown in b, c, d and e, respectively. The spectra are representatives of 2 runs of the experiments.

Figure 4 The Raman spectra of purified Se nanospheres from *Mc. capsulatus*

Figure 5 GC mass chromatograms of the liquid phase of the *Mc. capsulatus* (Bath) cultures amended with selenite (20 mg L^{-1}) at 4h (a) and 20h (b). The chromatograms were obtained by selecting the 80 m/z ion, and peak identification was achieved using the GC-MS library.

Figure 6 GC mass chromatograms of the headspace of the *Mc. capsulatus* (Bath) cultures amended with selenite (20 mg L^{-1}) at 4h (a) and 20h (b). The chromatograms were obtained by selecting the 80 m/z ion, and peak identification was achieved using the GC-MS library.

Scheme 1 A schematic diagram showing the reduction of selenite to methyl selenol with the subsequent formation of other selenium-containing species. The numbers donate the following: 1. reduction &methylation, 2. reduction & methylation, 3. polymerization, 4. exchange reactions.

Scheme 2 A schematic diagram showing the formation of methyl selenol, selenium particles and methylated derivatives.

Figure 1

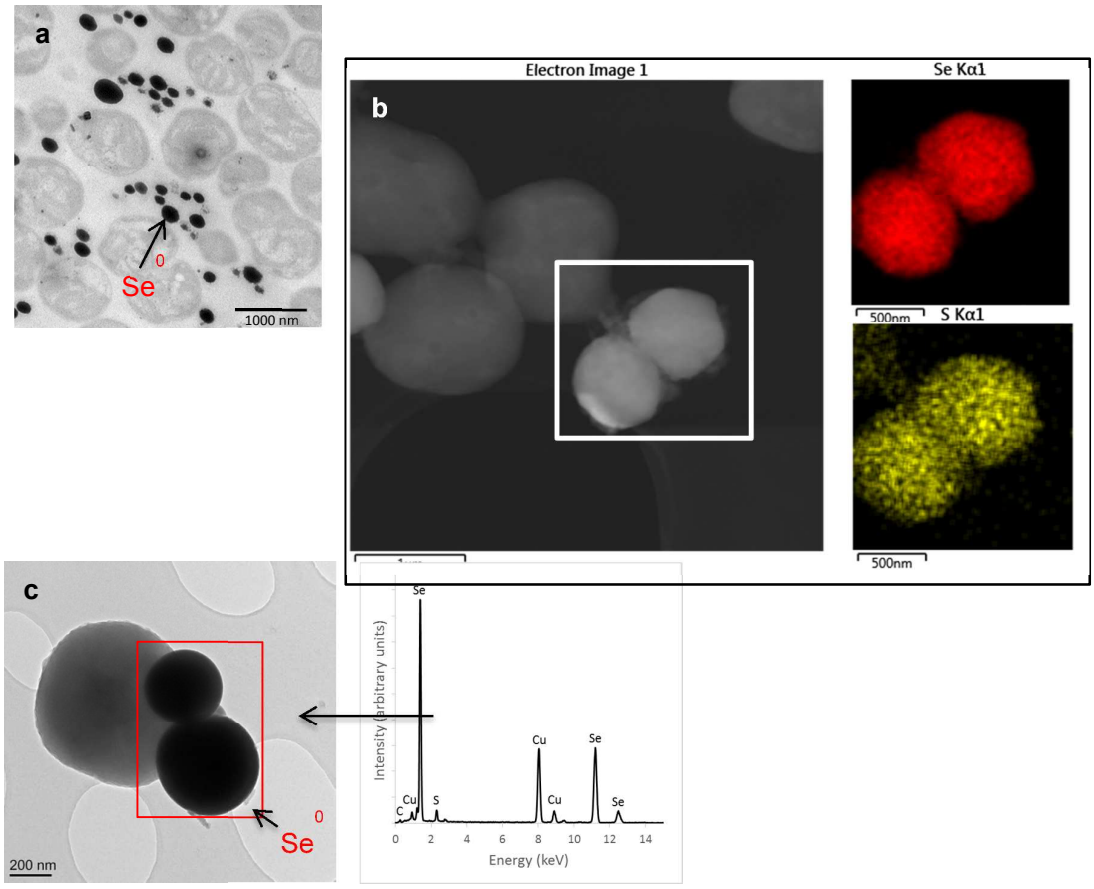

Figure2

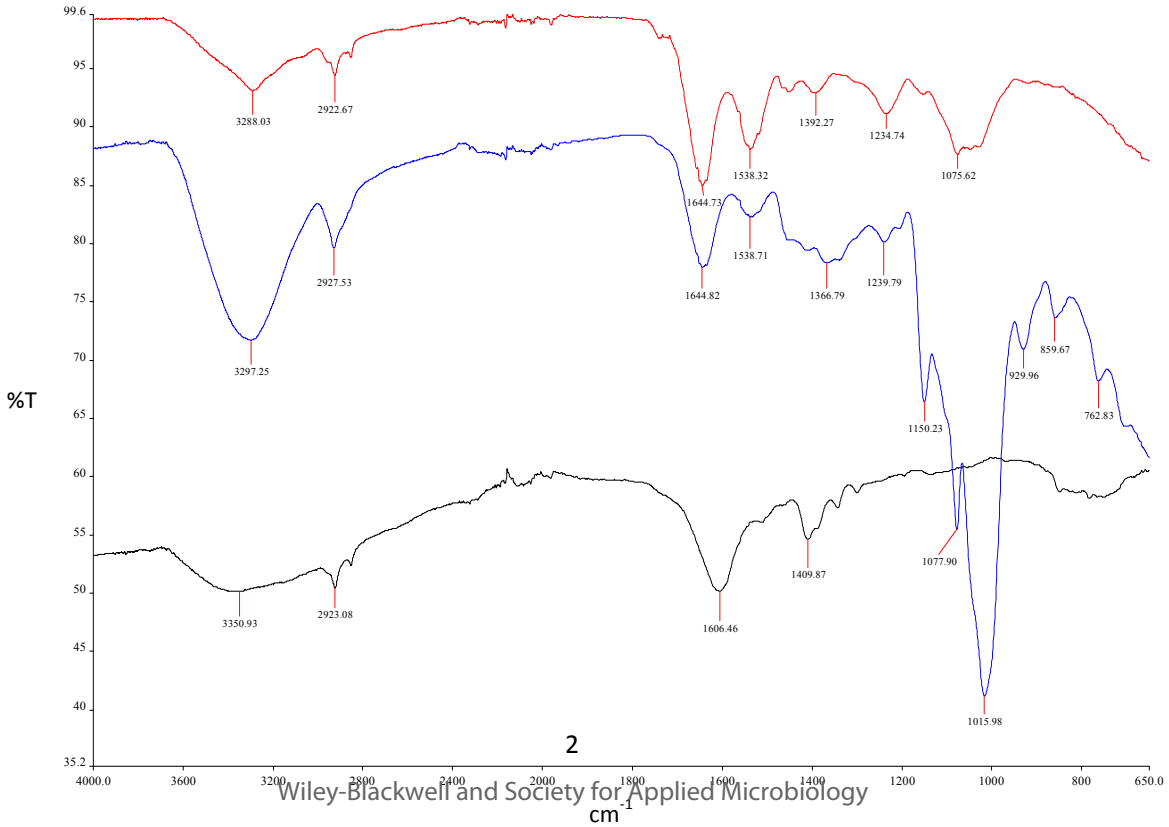

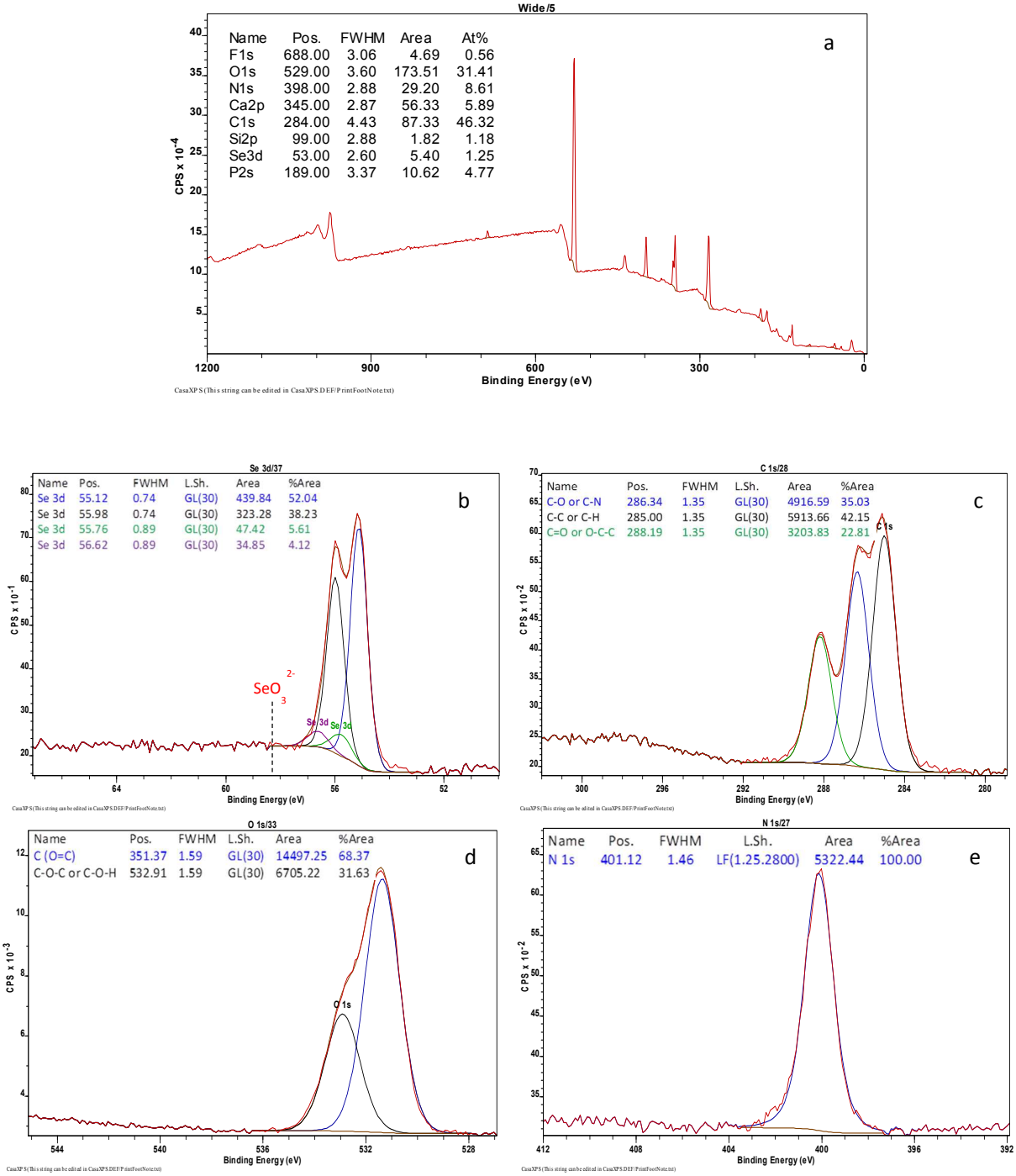
Wide/5
Name Pos. FWHM Area At%
F1s 688.00 3.06 4.69 0.56
O1s 529.00 3.60 173.51 31.41
N1s 398.00 2.88 29.20 8.61
Ca2p 345.00 2.87 56.33 5.89
C1s 284.00 4.43 87.33 46.32
Si2p 99.00 2.88 1.82 1.18
Se3d 53.00 2.60 5.40 1.25
P2s 189.00 3.37 10.62 4.77
a
CPS x 10-4
Binding Energy (eV)
Se 3d/37
Name Pos. FWHM L.Sh. Area %Area
Se 3d 55.12 0.74 GL(30) 439.84 52.04
Se 3d 55.98 0.74 GL(30) 323.28 38.23
Se 3d 55.76 0.89 GL(30) 47.42 5.61
Se 3d 56.62 0.89 GL(30) 34.85 4.12
b
SeO3 2-
Se 3d
Se 3d
CPS x 10-1
Binding Energy (eV)
C 1s/28
Name Pos. FWHM L.Sh. Area %Area
C-O or C-N 286.34 1.35 GL(30) 4916.59 35.03
C-C or C-H 285.00 1.35 GL(30) 5913.66 42.15
C=O or O-C-C 288.19 1.35 GL(30) 3203.83 22.81
c
C 1s
CPS x 10-2
Binding Energy (eV)
O 1s/33
Name Pos. FWHM L.Sh. Area %Area
C (O=C) 351.37 1.59 GL(30) 14497.25 68.37
C-O-C or C-O-H 532.91 1.59 GL(30) 6705.22 31.63
d
O 1s
CPS x 10-3
Binding Energy (eV)
N 1s/27
Name Pos. FWHM L.Sh. Area %Area
N 1s 401.12 1.46 LF(1.25.2800) 5322.44 100.00
e
CPS x 10-2
Binding Energy (eV)

Figure 3

Figure 4

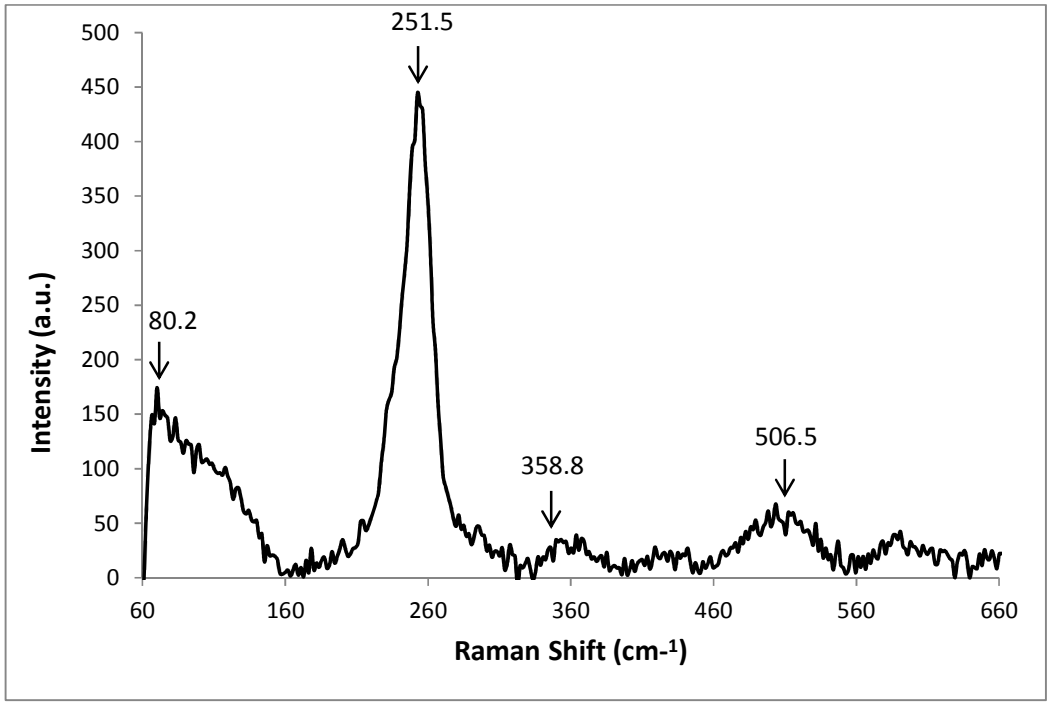
251.5
80.2
358.8
506.5
Intensity (a.u.)
Raman Shift (cm-1)
500
450
400
350
300
250
200
150
100
50
0
60
160
260
360
460
560
660

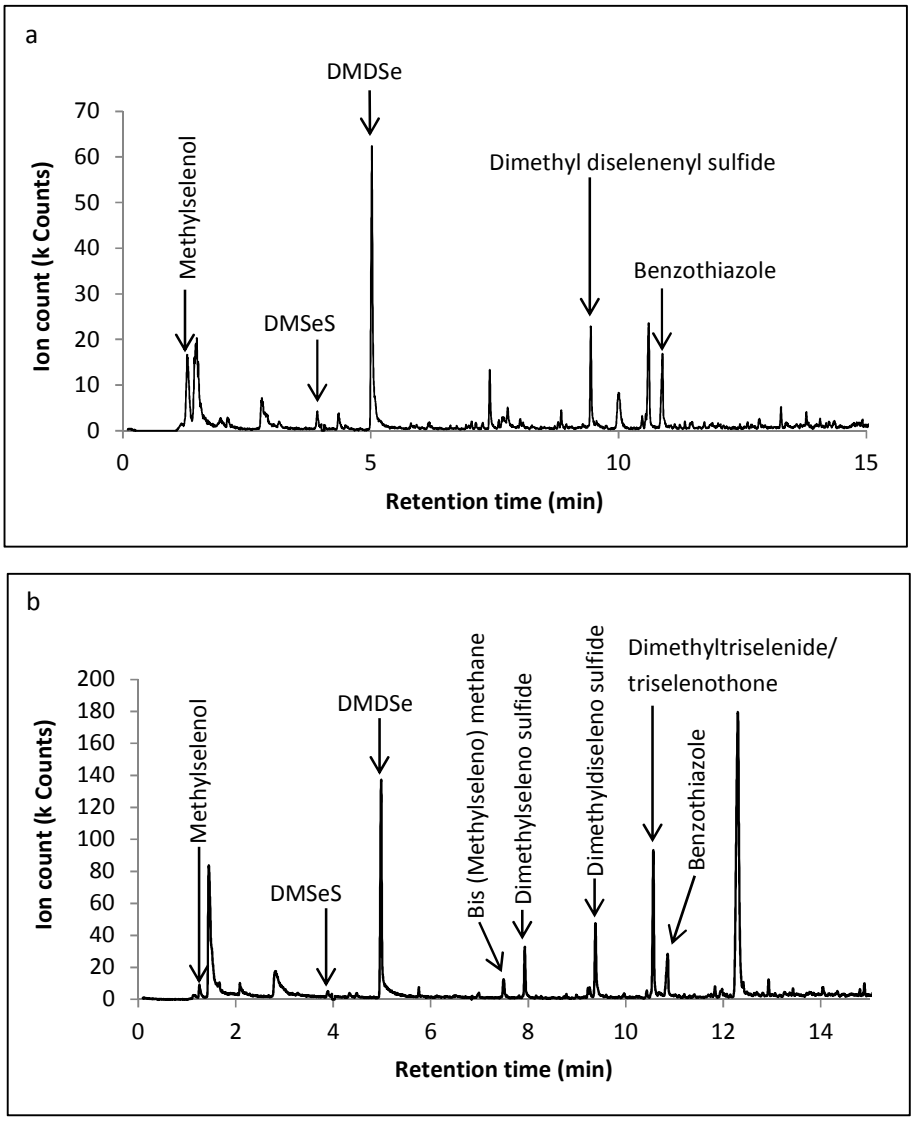
a
DMDSe
Methylselenol
Dimethyl diselenenyl sulfide
Benzothiazole
DMSeS
Ion count (k Counts)
Retention time (min)
b
Methylselenol
DMDSe
Bis (Methylseleno) methane
Dimethylseleno sulfide
Dimethyldiseleno sulfide
Dimethyltriselenide/
triselenothone
Benzothiazole
DMSeS
Ion count (k Counts)
Retention time (min)

Figure 5

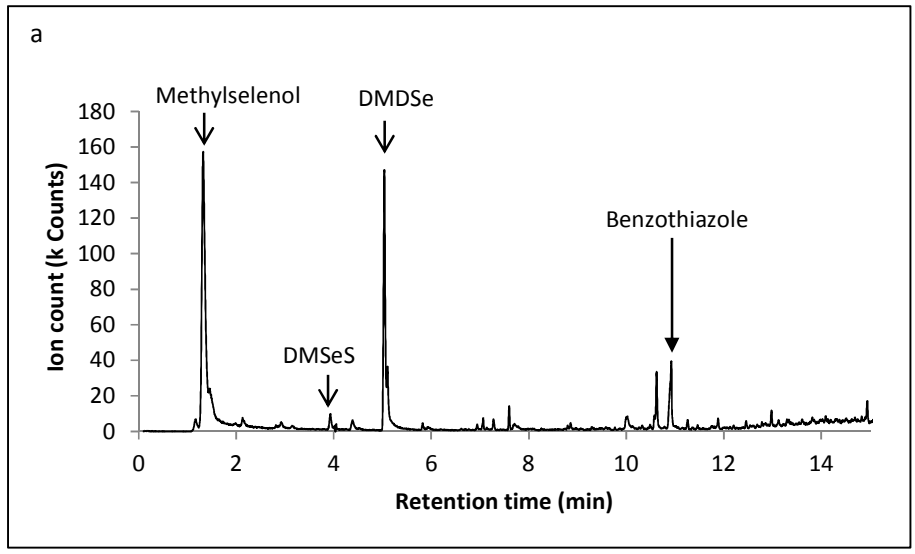
a
Methylselenol
DMDSe
Benzothiazole
DMSeS
Ion count (k Counts)
Retention time (min)
b
DMDSe
Methylselenol
Dimethyltriselenide/
triselenothone
Benzothiazole
DMSeS
Ion count (k Counts)
Retention time (min)

Figure 6

Scheme 1

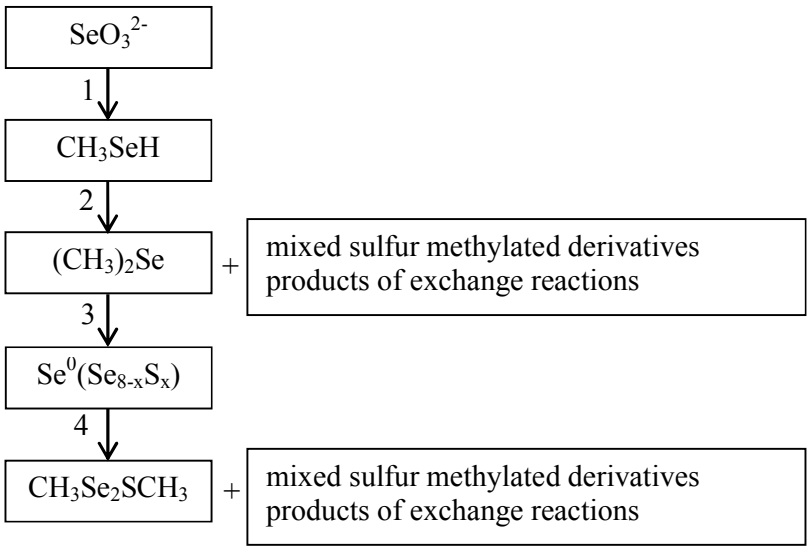

Scheme 2

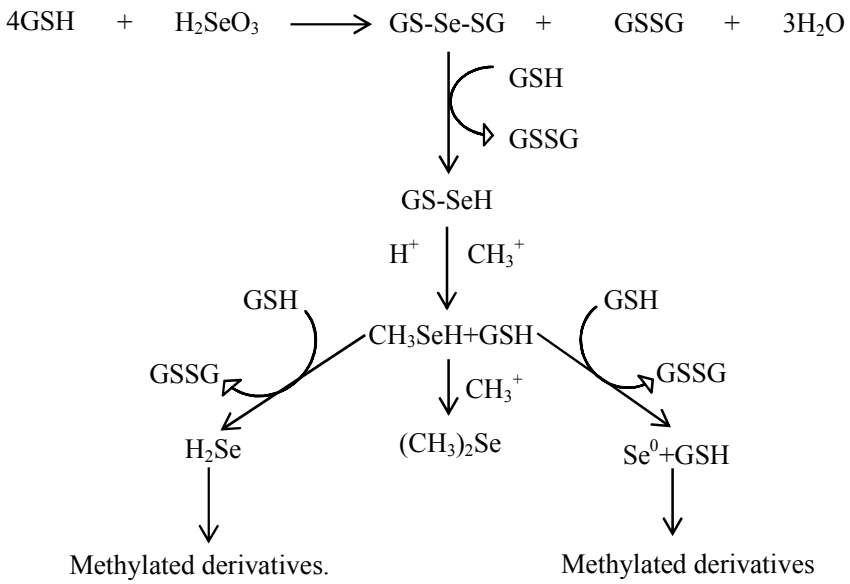

List of Tables

Table 1 Tentative assignments of main bands to the relevant functional groups (wavenumber, cm^{-1}) (Naumann *et al.*, 1995; Beekes *et al.*, 2007; Burattini *et al.*, 2008; Kamnev, 2008; Alvarez-Ordonez *et al.*, 2011; Ojeda & Dittrich, 2012; Kamnev *et al.*, 2017).

Sample	O—H; N—H (amide A in proteins)	C—H in $>CH_2$)	C=O (ester moiety)	Amide I (in proteins)	Carboxyl COO^-)	Amide II (in proteins)	$-CH_2$/$-CH_3$ (in proteins, lipids, polyesters, etc.)	C=O of COO^-)	C—O—C/C—C—O (in ester moieties)	Amide III / O-P=O	C-O, C—C , C—H, C—O—C in polysaccharides, and	Phosphoryl groups	"fingerprint region"
Cell biomass of *Mc. capsulatus*	3288	2922		1644		1538		1392		1234	1075		
SeNPs produced by *Mc. capsulatus*	3297	2927		1644		1538		1366		1239	1150	919	859
											1077		762
											1015		
Chem-SeNPs		2923			1606			1409					

Table 2. A summary of the selenium- and sulfur-containing species detected in the headspace and solution after 4h and 20h incubation of *Mc. capsulatus* (Bath) in selenite amended medium using sorptive extraction in conjunction TD-GC-MS analysis

Incubation Time		Species										
		Methyl selenol	DMSeS	DMDSe	Bis (Methylseleno) methane	Dimethyl selenosulfide	Dimethyl diselenenyl sulfide	Triselenothone/ Dimethyltriselenide	Benzothiazole	Diethyl sulfuxide	Propanesulfonyl	Dodecanethiol
In solution (selenite amended)	4 h	+	+	+	+	-	+	-	+	-	-	-
	20 h	+	+	+	+	+	+	+	+	+	-	-
In headspace (selenite amended)	4 h	+	+	+	-	-	-	-	+	-	-	-
	20 h	+	+	+	-	-	-	+	+	-	-	-
(Control)	20 h	-	-	-	-	-	-	-	+	-	+	+

+ = detected; - = unknown